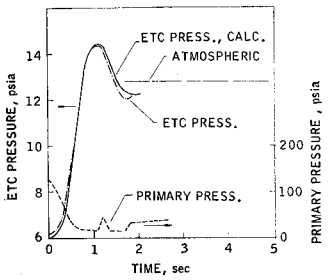

Fig. 6 Predicted and experimental nitrogen test results for ETS-1.

sistance and capacitive) is equated to the line terminal-pressure differences;

$$L\dot{m}/dt + R\dot{m} + 1/C\int\dot{m}/dt = P - \gamma \quad (8)$$

Clement and Johnson[1] obtain for the cell pressure the expression

$$P = \gamma + (P\infty - \gamma)[1 - e^{\alpha\sim t}(\cos\omega_t + \alpha/\omega \sin\omega_t)] \quad (9)$$

where

$$A = R/2\bar{L},\ \omega = 1/\bar{L}C - R^2/4\bar{L}^2 \quad (10)$$

In applying this method, the equivalent resistance of the duct is taken from the calculations of mass flow and pressure loss. The entrance and exit loss coefficients, K_e and K_c, respectively, are taken from London and Kays.[2]

For a $\frac{1}{8}$-scale program conducted at the Aerojet-General Corporation's Azusa Facility, the duct constants were calculated to be: α = 14.28 rad/sec, ω = 49.4 rad/sec. The ramp time required for the analysis was determined from gas pressure measurements either in the ejector manifold or the engine chamber. For the 10 tests, the average deviation from test data were 0.16 psi (8%) over-pressure and 0.036 sec (6%) in response time.

Five full-scale tests with N_2 without SGS were evaluated similarly. The test involved the sudden shutoff of the primary flow. The resistance of the duct with end effects included is R = 0.792 lbf-sec/lb-ft². The compliance is determined from the average change in pressure which results from the addition of 1 lb of gas, or by use of Eq. (5). With ETC volume = 5925 ft³, for gaseous N_2 at 520°R, the compliance (ETC + duct) is C = 0.2065 lb-ft²/lbf. Then with L = 0.2767 sec²/ft² (see Fig. 6), Eq. (11) gives (for A = 12.4 ft², L = 110 ft) α = 1.43 rad/sec, and ω = 3.93 rad/sec. The analysis shows (See Fig. 6) that ETC repressurizes to a maximum of 14.5 psia which is 1.7 psi higher than the ambient pressure of 12.8 psia at NRDS, reaching this pressure level 1.1 after the primary flow starts to decrease. The initial surge is followed by a series of pressure oscillations that are effectively damped in 5.5 sec (not shown).

The ETS-1 was also tested with He to provide a more realistic evaluation than was obtained from tests with N_2. The SGS flow was cut off as rapidly as practicable by shutting down the steam generators simultaneously. The test results are shown on Fig. 7. From the steam flow decay rate and the purge gas flow rate predicted ETC pressure is also shown on Fig. 7. It should be noted that the predicted ETC pressure peak occurs approximately the same time and has the same magnitude as the measured value.

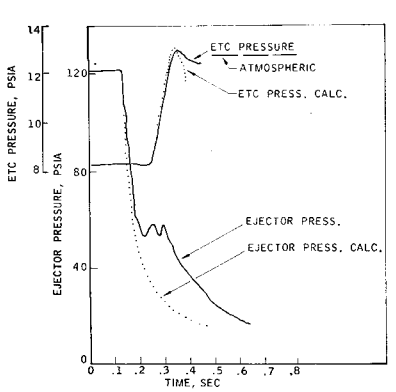

Fig. 7 Predicted and experimental helium test results for ETS-1.

In conclusion, the results of the analytical model agree well with the experimental data. The analytical predictions were confirmed by both visual observation and by using oxygen analyzers. The model can be used efficiently to modify either the design or the operating conditions for over-all system improvement.

References

[1] Clement, P. R. and Johnson, W. C., *Electrical Engineering*, McGraw-Hill, 1960, p. 265.

[2] Kays, W. M. and London, A. L., *Compact Heat Exchangers*, National Press, Palo Alto, Calif., 1955.

Gravity-Gradient Capture and Stability in an Eccentric Orbit

D. K. ANAND,* J. M. WHISNANT,† V. L. PISACANE,‡ AND M. STURMANIS†

The Johns Hopkins University, Silver Spring, Md.

Introduction

GRAVITY-GRADIENT stabilization of artificial satellites in near-circular orbits has been well demonstrated in the past. In this Note the capture and stabilization of a satellite in a highly eccentric orbit is considered. The satellite under consideration is Lidos, whose purpose is to yield geodetic information. It has an unsymmetrical inertia ellipsoid, four solar paddles arranged in a windmill fashion, a self-erecting boom with end mass, permeable rods for hysteretic damping and a dipole magnet for performing inversion maneuvers in case the satellite is initially captured in the undesired mode.

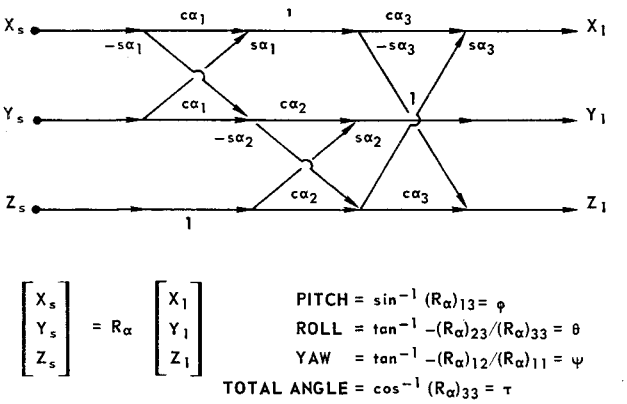

Fig. 1 Coordinate transformation and angle representation.

Presented as Paper 69-921 at the AIAA/AAS Astrodynamics Conference, Princeton, N.J., August 20–22, 1969; submitted August 12, 1969; revision received September 10, 1969. This work was done under Navy Contract NOw-62-0604-c.

* Senior Staff, Space Research and Analysis Branch, Applied Physics Laboratory; also Associate Professor of Mechanical Engineering, University of Maryland. Member AIAA.

† Associate Mathematician, Space Research and Analysis Branch, Applied Physics Laboratory.

‡ Supervisor, Theory Project, Space Research and Analysis Branch, Applied Physics Laboratory. Member AIAA.

It is to be gravity-gradient stabilized in an orbit having an eccentricity of 0.2 and a semimajor axis of 1.45 earth radii.

Satellite oscillations in the plane of an elliptic orbit are described[1,2] by the following differential equation:

$$(1 + e\cos\nu)\frac{d^2\varphi}{d\nu^2} - 2e\sin\nu\frac{d\varphi}{d\nu} + \alpha\sin\varphi\cos\varphi = 2e\sin\nu$$

where e is the eccentricity, $\alpha = 3[(I_x - I_z)/I_y]$, φ is the pitch libration angle measured from the local vertical, and ν is the true anomaly. This equation has been investigated by researchers using numerical integration and phase space representation. The stable region is symmetrical about the local vertical at $\nu = 0$ and π for all e and $\alpha \approx 3$.[1,2] The region of stability becomes skewed as ν varies from 0 to π to 2π, and it shrinks as e is increased, until e reaches 0.355, when gravity-gradient stabilization is no longer possible for any configuration.

Consider a satellite having $\alpha \approx 3$ in an orbit with 0.2 eccentricity. The resulting pitch oscillations have an amplitude of 0.26 rad (initial conditions of $\varphi = 0$, $\dot{\varphi} = 0.74$ at $\nu = 0$). An approximation of this result can be obtained by solving the Mathieu equation.[3-5] Note that φ is in degrees and $\dot{\varphi}$ is nondimensionalized by $\dot{\nu}(\varphi)$.

It is not sufficient to consider only eccentricity that primarily affects pitch librations. Perturbations due to thermal bending, solar radiation pressure, and magnetic torques must be included. Solar radiation pressure is principally felt in roll and yaw; the forcing function in roll has a component with twice orbital frequency, and since the natural frequency is also the same, resonant conditions tend to be set with a particular combination of orbit elements and solar aspect.[6] This effect, coupled with the eccentricity effect gives rise to large roll motion, and although the pitch motion is within stable bounds, tumbling in roll can occur.

The theory for the attitude motion of a spacecraft has been developed using the Lagrangian and in a form suitable for computer simulation. External forces and torques are included in the simulation. The solar effect consists of both thermal distortion of the stabilizing booms and a solar radiation pressure torque on the deformed spacecraft. The gravitational torque not only provides the basic stabilizing mechanism but also introduces attitude perturbations through the eccentricity of the orbit. The magnetic torques are simulated using a geomagnetic field model written in terms of spherical harmonics. An analytical model for hysteretic damping has been developed and is included in the simulation.[7]

Attitude Simulation

The coordinate transformation and system used to define pitch, roll, and yaw angles are shown in Fig. 1. The results of the simulation are presented as plots of these three angles and the total off-vertical angle as a function of time for various combinations of physical parameters. Table 1 presents the physical properties common to all runs.

Table 1 Physical parameters

Orbit parameters: $a = 1.45$, $e = 0.1992$, $i = 96°$, $\Omega = 0°$, $\omega = 0°$, 190° (sun's right ascension and declination were zero)	
Main Spacecraft: $M = 135.6$ lb, $I_x = I_y = 8.7$ slug ft^2, $I_z = 17.0$ slug ft^2	
Equivalent cylinder = 25.4-cm radius, 31.0 cm high; surface reflectivity = 0.8	
Booms: $m = 0.0154$ lb/ft	
Radius of curvature due to thermal bending	= 1500 ft
Surface reflectivity	= 0.88
Diameter	= 1.27 cm
End mass: $M = 5.0$ lb, area = 268 cm^2	
Solar paddles: area = 4280 cm^2, surface reflectivity = 0.25	
Magnetic rods: volume = 17.56 cm^3, diameter = 0.275 cm; material, AEM 4750	

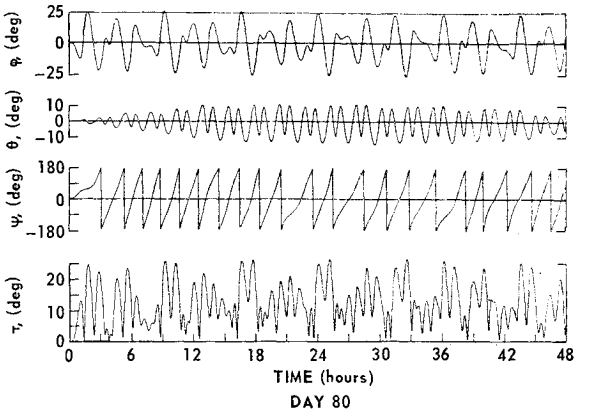

Fig. 2 Steady-state oscillations for 60-ft boom with 5-lb end mass.

The effect of eccentricity alone is felt principally in pitch motion. The peak amplitude is about 24° in pitch with no oscillations in roll and yaw.

Different orbits were studied to obtain the most adverse set of conditions that would yield an upper bound on attitude motion.[8] It was found that the orbit giving resonant conditions in roll was such an orbit, and the rest of this study is based on it. A parametric steady-state study was conducted which determined that the combination of 60-ft boom length and 5-lb end mass was optimum. The result of this simulation is shown in Fig. 2. The yaw motion occurs since the solar paddles are arranged in a windmill fashion. The energy associated with yaw motion, if transferred, is capable of causing a 6° roll motion. From an attitude stability viewpoint such performance is acceptable. The benefit to be derived from the yaw motion is the smoothing of thermal fluctuations of the satellite. External perturbations cause no substantial change in pitch, although roll oscillations increase to about 10°, and the satellite rotates in yaw at the rate of one or two revolutions per orbit.

Transient response to an initial condition in pitch is shown in Fig. 3 for 3 cases: two hysteretic damping rods 57 in. long, four 57-in. rods, and a General Electric magnetically anchored damper (damping constant of 8×10^4 dyne-cm-sec/rad). Although the results with the GE damper are somewhat superior than those obtained by magnetic hysteresis damping, scheduling limitations dictated use of the latter. Inversion maneuvers were simulated using a dipole magnet pointed in a direction opposite to the boom. Satisfactory results were obtained using a magnet of strength 44,000 pole-cms.

Stability and Capture

It is important to know the stability region before attempting to capture the satellite. For orbits with $\epsilon < 0.1$, the point $\varphi = 0$, $\dot{\varphi} = -1$ is always within the stable region of the phase plane. Therefore, if the moment of inertia is adequately increased anywhere in the orbit, provided φ is within stable limits, then $\dot{\varphi} \approx -1$ and the satellite is captured in the gravity-gradient mode. This maneuver has been done many times and is well understood.

However, when $e > 0.1$, the foregoing procedure does not always insure capture, since $\dot{\varphi} = -1$ is out of the stable region for certain values of the true anomaly.[1,2] Specifically, when $e = 0.2$, the point $\dot{\varphi} = -1$ is not inside the stable region anywhere in the orbit except for a small time around apogee. This is shown in the stroboscopic study of Fig. 4. Additionally, the study of the regions of stability with different parameters and including perturbing forces is reported elsewhere.[9] It suffices to note, however, that the region of stability obtained is larger than that reported before.

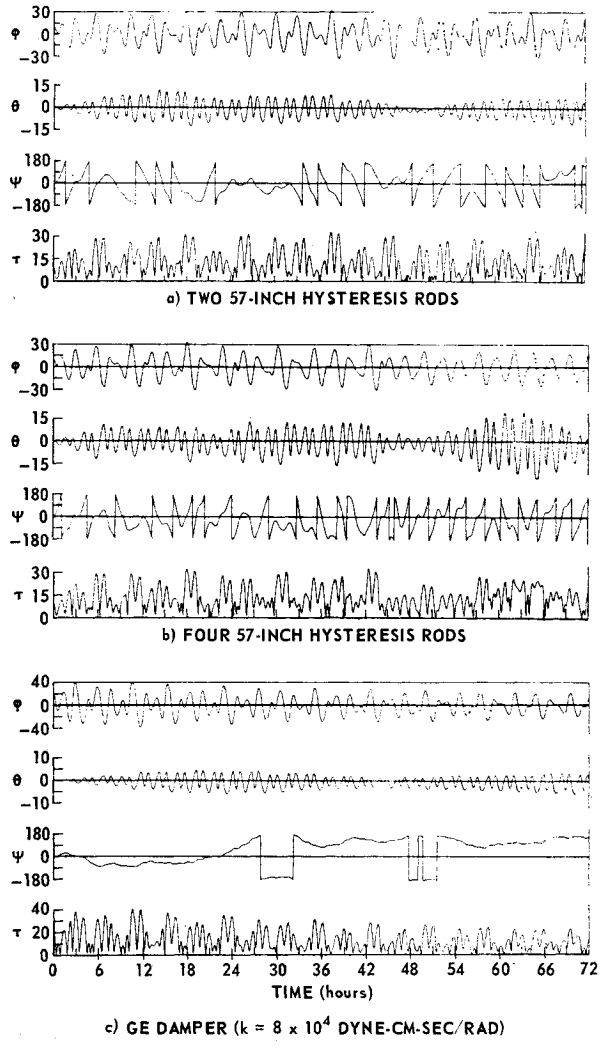

Fig. 3 Transient responses for 60-ft boom and 5-lb end mass, 80 days.

Because of the existence of perturbations, the exact determination of the region around $\dot{\varphi} = -1$ is difficult. Therefore, to effect satellite capture anywhere in the orbit, the satellite must be maneuvered into the stable region. The maneuvering is achieved by using an electromagnet. The satellite is magnetically stabilized, and the boom is erected while the electromagnet is still on. The magnetic torque opposes the gravitational torque and drives the satellite into the stable region, at which time the electromagnet is turned off and capture is effected.

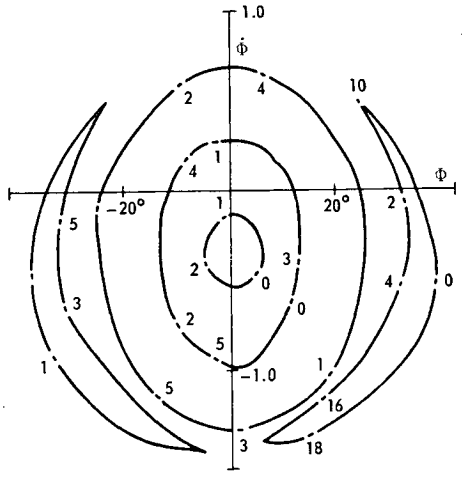

Fig. 4 Stroboscopic study at $\nu = \pi$ for an eccentricity of 0.2.

The stability regions for $290° \leq \nu \leq 310°$, $310° \leq \nu \leq 330°$, and $300° \leq \nu \leq 320°$ are shown in Fig. 5 for the stable initial conditions, $\varphi = 18°$, $\dot{\varphi} = 0$ at perigee. The equations of attitude motion are now integrated beginning at $\nu = 262°$ and with different initial conditions. It is assumed here that the satellite is magnetically stabilized, the boom for appropriate inertia is erected, and the electromagnet is on. The resulting trajectories (φ and $\dot{\varphi}$ with time as parameter) are superimposed on the stability charts. Trajectories obtained with initial conditions of $-10°$, $+10°$, $0°$, and zero rates in each case are shown in Figs. 5a, 5b, and 5c, respectively.

It is seen that the attitude motion is driven inside the stable region and stays inside for ~8 min. If the electromagnet and all perturbing effects are turned off during this time interval, the satellite is captured. The exact locations of the stability regions and attitude trajectories depend

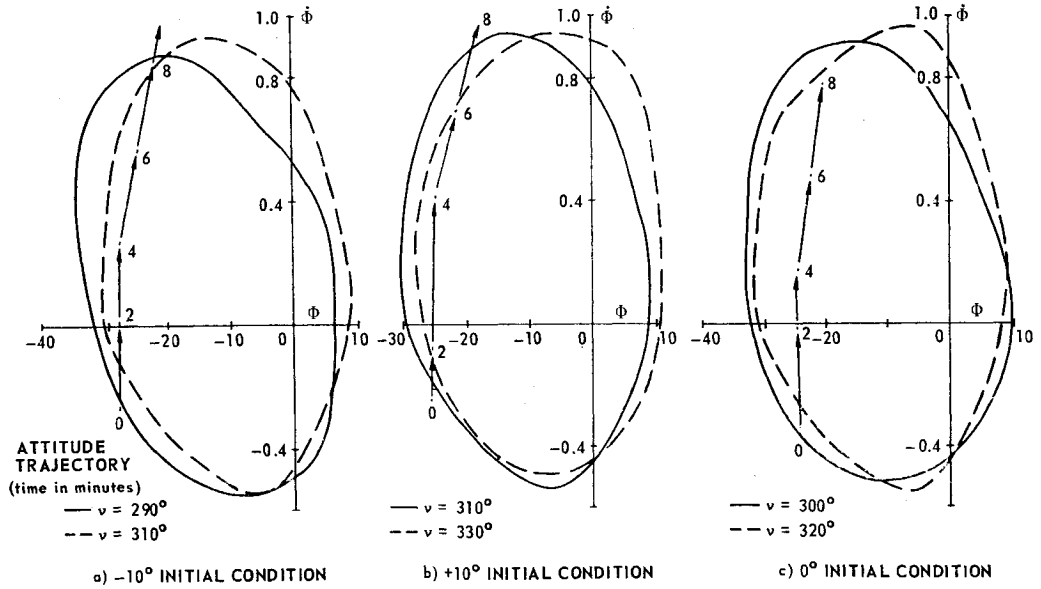

Fig. 5 Attitude trajectories, of different initial conditions at $\nu = 262°$, superimposed on the stability region for eccentricity of 0.2.

upon ν and the initial conditions applied at $\nu = \nu_0$. In any practical situation, this must be a real-time operation.

References

[1] Zlatoustov, U. A. et al., "Investigation of Satellite Oscillations in the Plane of an Elliptic Orbit," *Proceedings of the 11th International Congress of Applied Mechanics*, Springer-Verlag, Berlin, 1966, pp. 436–439.

[2] Brereton, R. C. and Modi, V. J., "On the Stability of Planar Librations of a Dumbbell Satellite in an Elliptic Orbit," *Journal of the Royal Aeronautical Society*, Vol. 70, No. 672, Dec. 1966, pp. 1098–1102.

[3] Graham, D. and McRuer, D., *Analysis of Nonlinear Control Systems*, Wiley, New York, 1961, p. 70.

[4] Frick, R. H. and Garber, T. B., "General Equations of a Motion of a Satellite in a Gravitational Gradient Field," Rept. RM-2527, Dec. 1959, The Rand Corp.

[5] Baker, R. M. L., "Librations on a Slightly Eccentric Orbit," *ARS Journal*, Vol. 30, No. 1, Jan. 1960, pp. 124–126.

[6] Whisnant, J. M. and Anand, D. K., "Roll Resonance for a Gravity-Gradient Satellite," *Journal of Spacecraft and Rockets*, Vol. 5, No. 6, June 1968, pp. 743–744.

[7] Whisnant, J. M. et al., "The Dynamic Modeling of Hysteresis and Application to Damping of Spacecraft Librations," AIAA Paper 69-833, Princeton, N.J., 1969.

[8] Anand, D. K., Whisnant, J. M., and Sturmanis, M., "The Capture and Stability of a Gravity-Gradient Satellite in an Eccentric Orbit," Rept. TG-1028, Aug. 1968, Applied Physics Lab., The Johns Hopkins Univ., Silver Spring, Md.

[9] Anand, D. K., Yuhasz, R. S., and Whisnant, J. M., "Further Comments on Attitude Motion in an Eccentric Orbit," TM, Applied Physics Lab., The Johns Hopkins Univ., Silver Spring, Md., in preparation.

Prediction of Flight Performance of a Throttling, Ablative Rocket Engine

ROBERT D. BAKER*

Systems Group of TRW Inc., Redondo Beach, Calif.

Nomenclature

A = cross-sectional area, in.^{2}
C,D,E = empirical constants
C_f = nozzle thrust coefficient, dimensionless
C^* = characteristic velocity, fps
F = engine vacuum thrust, lbf
g = mass equivalence = 32.174 lbm/slug
I_{sp} = engine specific impulse, lbf-sec/lbm
K = hydraulic conductance
L^* = chamber characteristic length, ft
M = mass of spacecraft, slugs
P = pressure, psia
ΔP = injector pressure drop, psid
r = radial distance, ft
Rm = mixture ratio, dimensionless
S = throttle position, percent of maximum
T = temperature, °R
t = measured burn time, sec
T_{120} = time required to erode a fiberglass nozzle throat 20%, sec
ΔV = characteristic velocity, fps
$\dot{w}$ = propellant flowrate, lbm/sec
α = injector momentum ratio, oxidizer/fuel
β = ratio of nozzle stagnation pressure to chamber pressure, dimensionless
θ = angular displacement, radians
λ = combustion chamber gas velocity function
μ = gravitation constant, ft^3/sec^2
ρ = fluid density, lbm/ft^3
τ = time dummy variable, sec
ϕ = thrust vector angle from local horizontal, deg
Ψ = error function, dimensionless

Subscripts

t = nozzle throat, total
o = original or initial, oxidizer
i = vector index, interface, station in flow system
c = chamber
e = engine, combustion gas
f = fuel
n = nozzle

Presented as Paper 69-452 at the AIAA 5th Propulsion Joint Specialist Conference, U.S. Air Force Academy, Colo., June 9–13, 1969; submitted June 4, 1969; revision received September 2 ,1969.

* Head, Flight Systems Section, Professional Engineer, Senior Lecturer in Engineering, University of Southern Calif. Member AIAA.

Introduction

IN simulating the performance of a throttling, ablative rocket engine system, variations of performance with respect to the engine throttle position must be considered in addition to performance deviations produced by off-nominal engine interface conditions and throat erosion. Performance parameters such as vehicle ΔV gain, delivered impulse, and propellant consumption are dependent upon the throttle time profile employed during the mission as well as the initial performance measured during acceptance tests of the engine. If the engine is to be used on a soft-landing mission, it will be necessary to augment the engine performance characterization with the actual dynamic constraints of the flight path. Such a capability has been developed at TRW Systems to simulate the performance of the lunar module descent engine (LMDE) executing a lunar landing mission (LLM).

Discussion

Analysis can be carried out assuming a fixed throttle-time profile representing a nominal mission or the model can be augmented with the actual dynamic equations describing the accelerations experienced while transiting a conservative centralized inverse square force field. Usual simplifying assumptions for an LLM are: spherical moon without gravitational perturbations, two-dimensional flight in the equatorial plane, and no drag. The equations of motion for this problem in polar coordinates are

$$r\ddot{\theta} + (F/M)\cos\phi + 2\dot{r}\dot{\theta} = 0 \quad (1)$$

$$\ddot{r} - r\dot{\theta}^2 + (F/M)\sin\phi + \mu/r^2 = 0 \quad (2)$$

Figure 1 illustrates the directions of these acceleration terms. The targeted speed and altitude parameters then act as the constraints for the mission. To meet these constraints in the nominal case the LMDE throttle-time profile is as shown in Fig. 2. The remainder of the propulsion system simulation model can be constructed in either one of two ways, by use of an influence coefficient model or a nonlinear model.

Influence Coefficient Method

The most compact and simplest form is to take a linear approach wherein the basic external performance parameters (P_c,Rm,F,$\dot{w}_t$, and hence I_{sp}) are tabulated against throttle position for nominal engine operation. Critical performance parameters are then determined in the nominal case by interpolating the table based on the required throttle position. Off-nominal conditions are accounted for by the use of linear influence factors on the tabulated parameters. Off-nominal conditions† are considered to be produced by external factors.

The accelerations required to meet the speed and altitude constraints shown in Fig. 1 are augmented with the instantaneous mass of the vehicle and the required throttle position

† Such as off-nominal interface pressure, temperatures, gas absorption within propellants, etc.